Anion Surfactant-Tailored Electric Double-Layer: Toward Higher Faradaic Efficiency in Acidic CO_2 Electrolysis

Zheng Zhang [a,b], Lei Tang [a], Yihua Zhu [b], Wangxin Ge [a,*], Hongliang Jiang [a,*], and Chunzhong Li [a,b,*]

[a]Key Laboratory for Ultrafine Materials of Ministry of Education, School of Chemical Engineering, East China University of Science and Technology, Shanghai 200237, China

[b]Shanghai Engineering Research Center of Hierarchical Nanomaterials, School of Materials Science and Engineering, East China University of Science and Technology, Shanghai 200237, China

*Corresponding Author

E−mail address: gwx@ecust.edu.cn (Wangxin Ge); jhlworld@ecust.edu.cn (Hongliang Jiang); czli@ecust.edu.cn and czlilab@sjtu.edu.cn (Chunzhong Li)

1. Chemicals and Materials.

Sulfonate anionic surfactants with varying alkyl chain lengths: Sodium butyl sulfate (SBS, 98%), Sodium octyl sulfate (SOS, 98%), Sodium dodecyl sulfate (SDS, 98%) and Sodium Hexadecyl sulfate (SHS, 98%), Lauryl alcohol (LA), Potassium sulfate (K_2SO_4, 99.7%), Ag NPs (99.5%, 60–120 nm) and Nafion perfluorinated resin solution (5 wt% in a mixture of lower aliphatic alcohols and water) were supplied by Macklin. Sulfuric acid (H_2SO_4, 95–97%) was procured from Sigma-Aldrich. Tin powder (99.99%, metals basis) and Indium oxide (99.99%, metals basis, powder) procured from Aladdin. Deionized water (18.25 MΩ cm) was employed in all experiments.

2. Supplementary Figures:

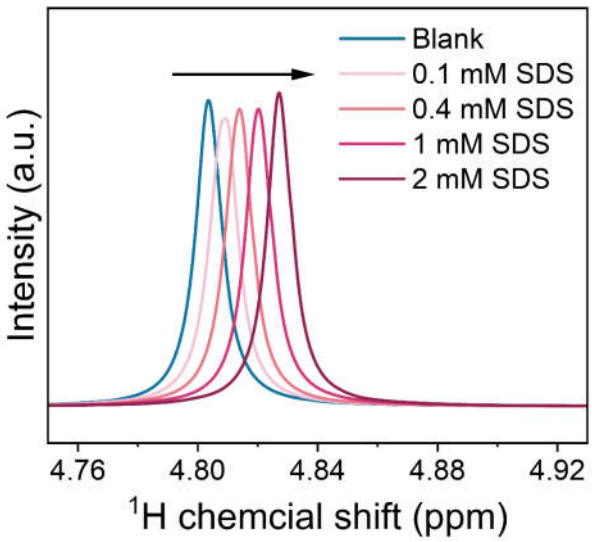

Figure S1. ^{1}H NMR spectra of 0.1 M H_2SO_4 + 0.2 M K_2SO_4 electrolyte with different concentrations of SDS.

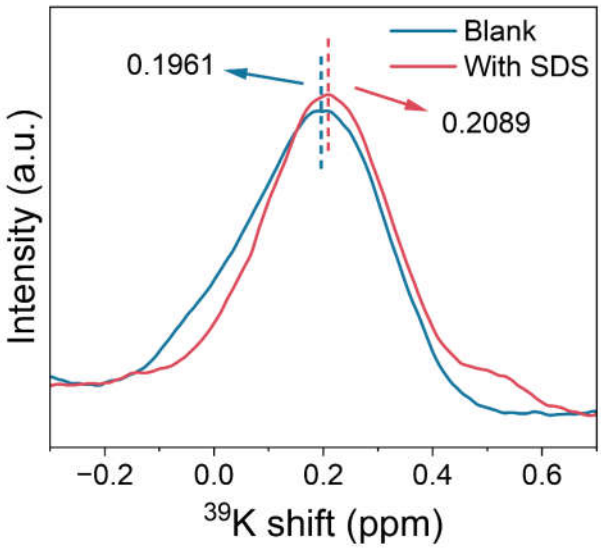

Figure S2. ^{39}K NMR spectra of 0.1 M H_2SO_4 + 0.2 M K_2SO_4 electrolyte without/with 0.4 mM SDS.

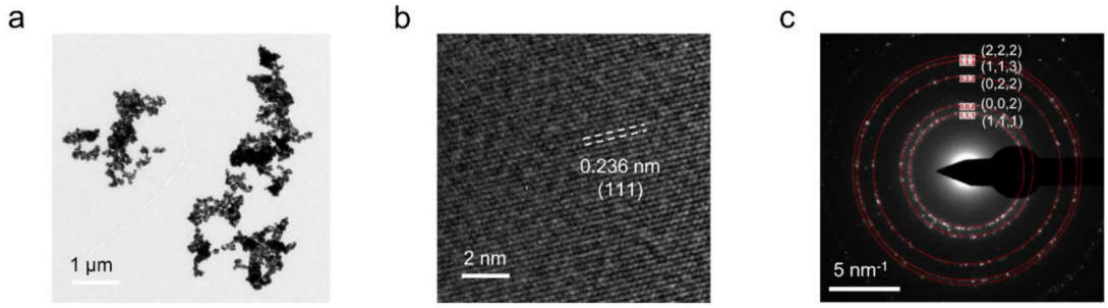

Figure S3. (**a**) TEM, (**b**) HRTEM and (**c**) SAED images of Ag NPs.

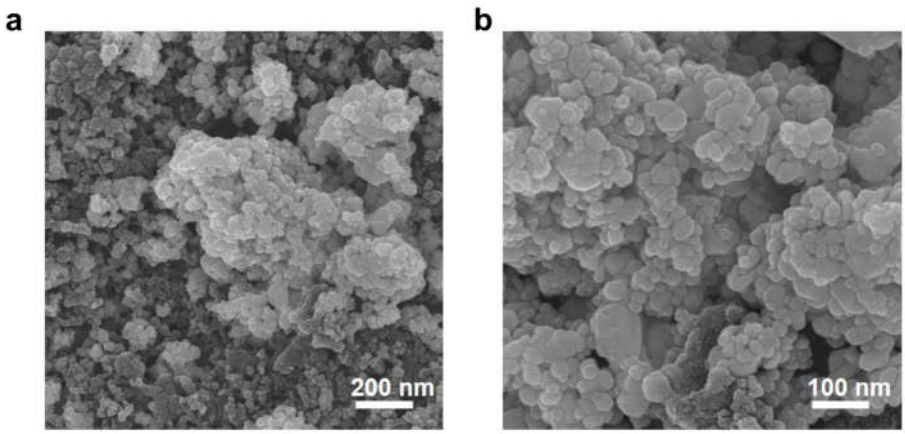

Figure S4. SEM images of Ag NPs.

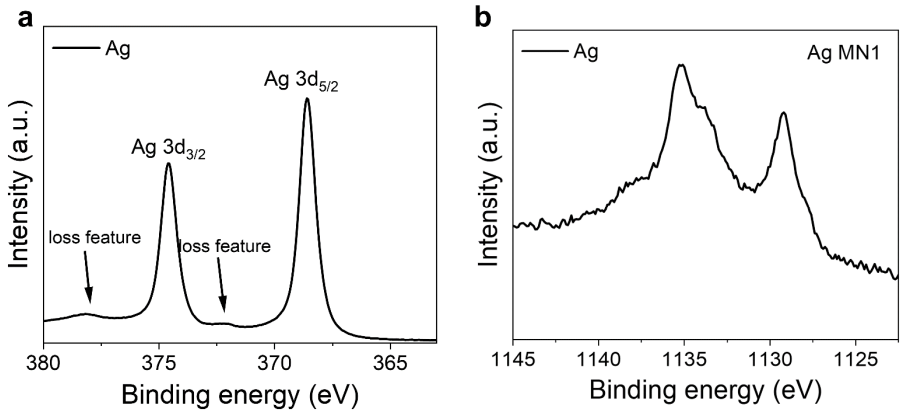

Figure S5. (a) XPS and **(b)** Auger spectra of Ag NPs.

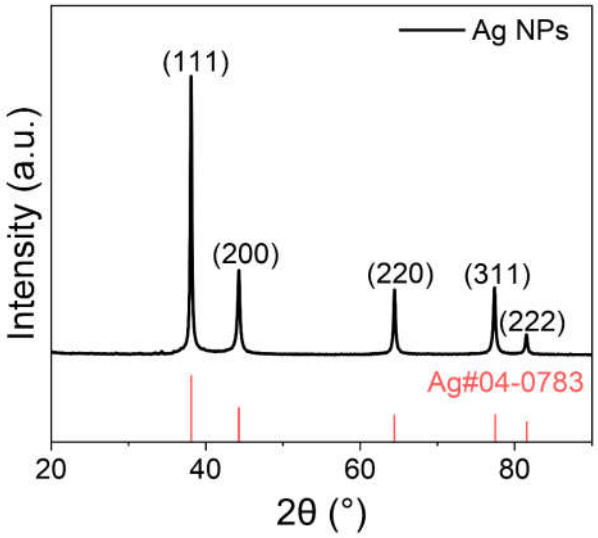

Figure S6. XRD pattern of Ag NPs.

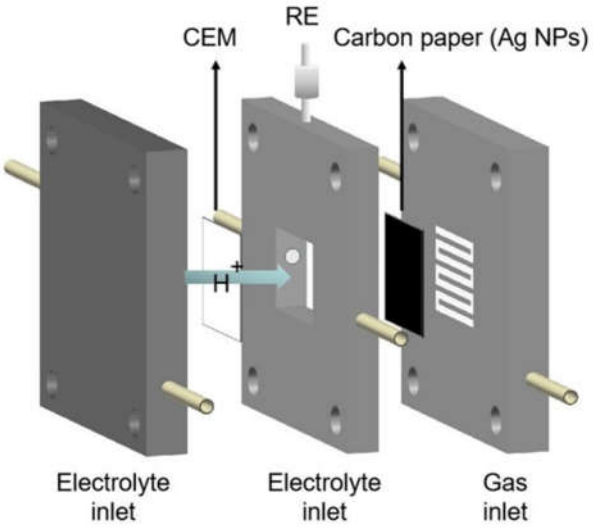

Figure S7. Schematic of the flow cell electrolyzer.

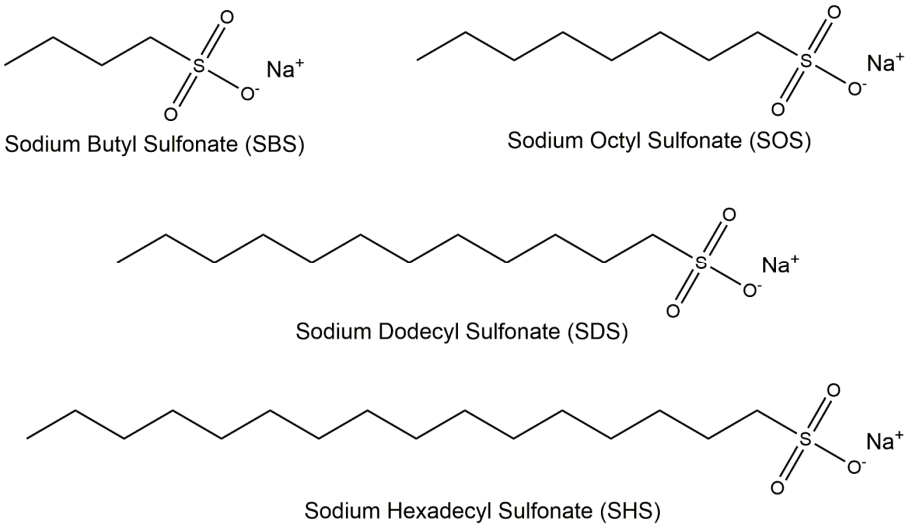

Figure S8. Structural formulae of different anionic surfactants.

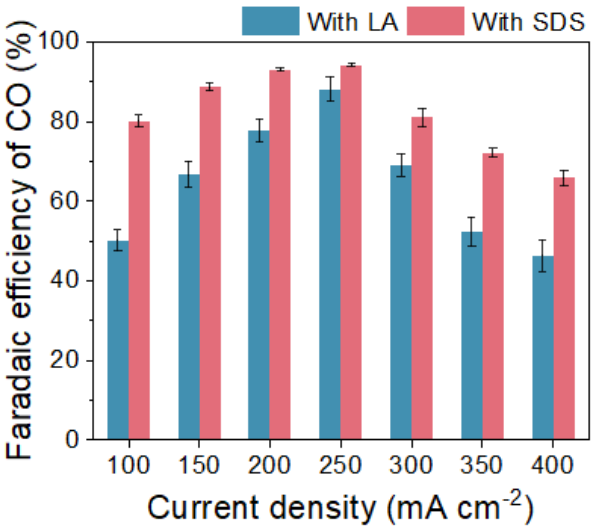

Figure S9. FE of CO in 0.1 M H_2SO_4 + 0.2 M K_2SO_4 electrolytes with SDS and LA in flow cell.

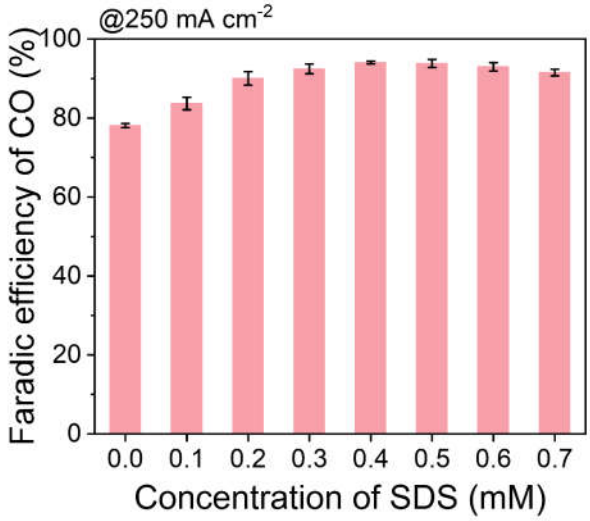

Figure S10. FE of CO in 0.1 M H_2SO_4 + 0.2 M K_2SO_4 electrolytes without and with different concentration of SDS at 250 mA cm^{-2} in flow cell.

Increasing the concentration of SDS from 0.1 mM to 0.4 mM, the faradaic efficiency of CO gradually increases, indicating that a certain content of SDS is necessary for performance enhancement. As the surfactant concentration further increased, there is a slight decrease in CO selectivity, which we speculate results from micelle-induced bubbles generated by high concentrations of surfactants that interfere with the electrolysis process.

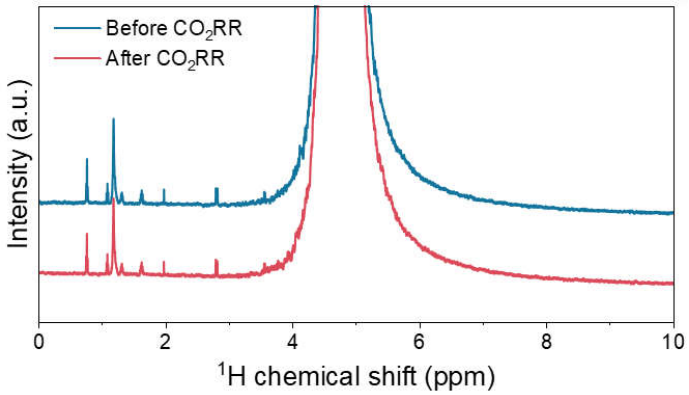

Figure S11. ^{1}H-NMR spectra of SDS-containing electrolyte before and after CO_2RR.

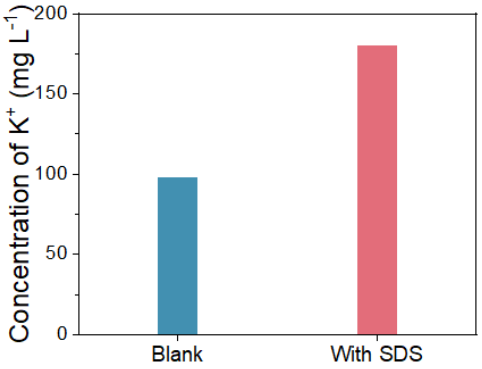

Figure S12. Comparison of the adsorbed-K^+ concentration in electrolytes with and without SDS.

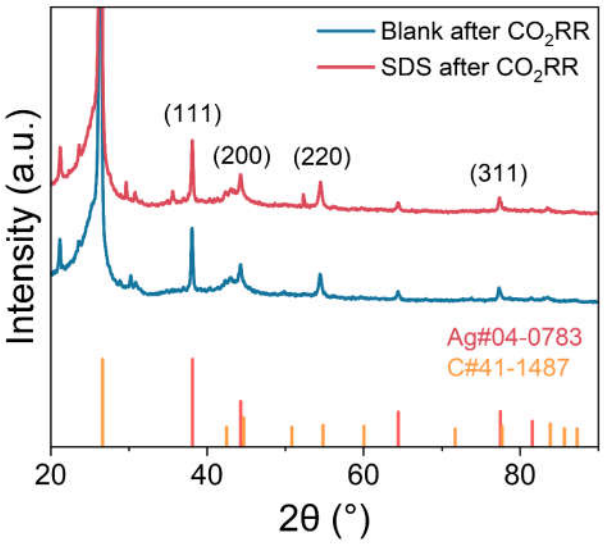

Figure S13. XRD patterns of Ag-GDE electrode after CO_2RR in two electrolyte systems.

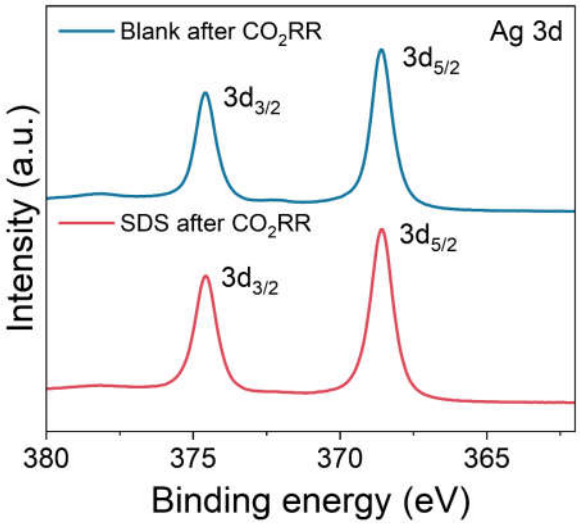

Figure S14. XPS spectral of Ag-GDE electrode after CO_2RR in two electrolyte systems.

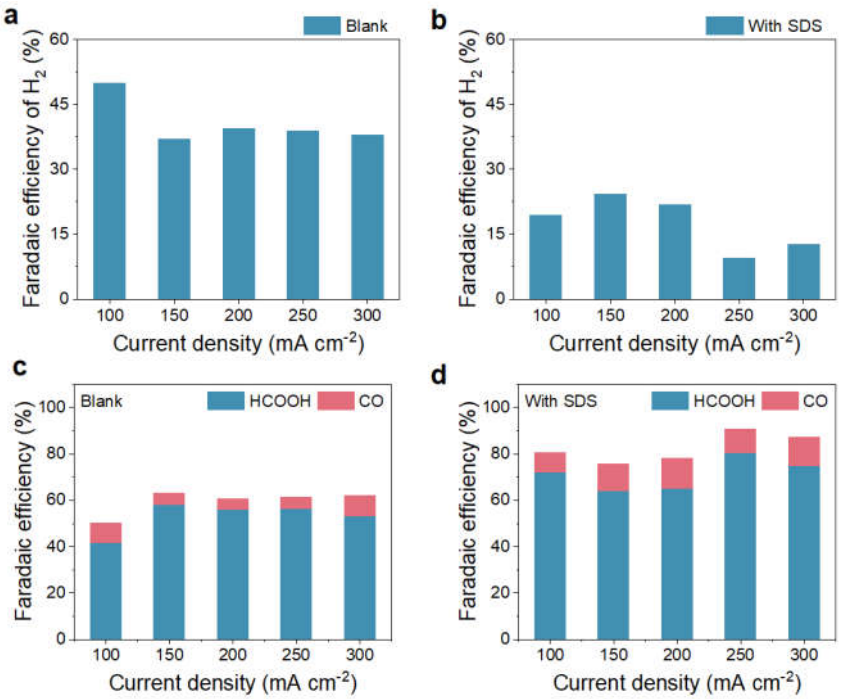

Figure S15. FEs in 0.1 M H_2SO_4 + 0.2 M K_2SO_4 electrolytes with SDS and LA in flow cell with Sn catalyst.

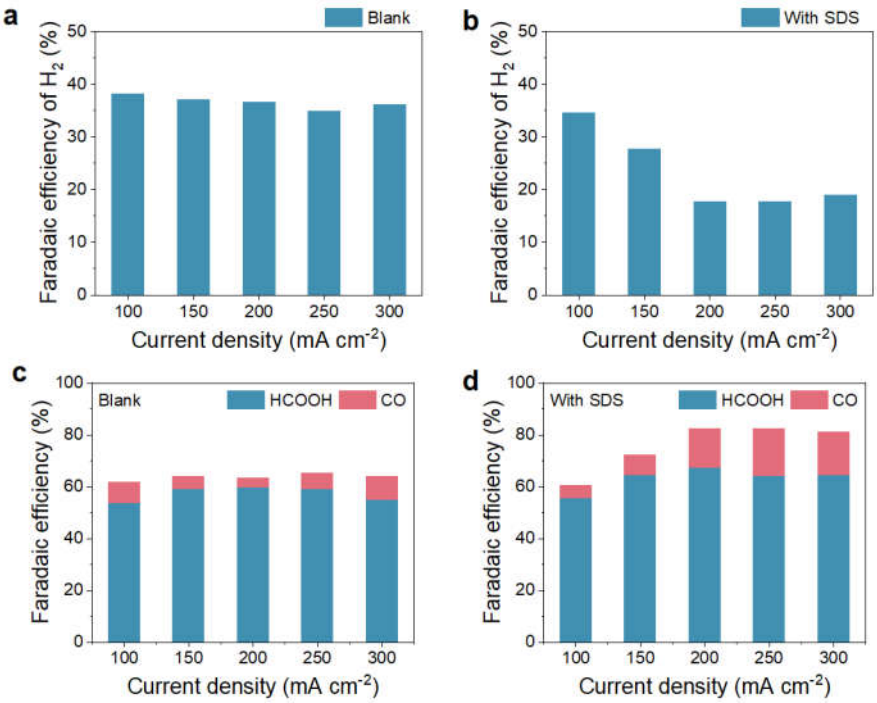

Figure S16. FEs in 0.1 M H_2SO_4 + 0.2 M K_2SO_4 electrolytes with SDS and LA in flow cell with In_2O_3 catalyst.

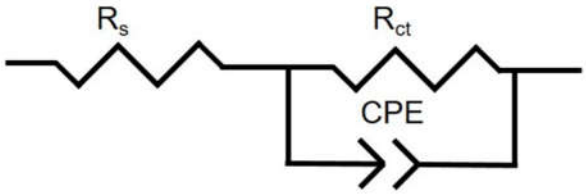

Figure S17. The used the equivalent circuit of all systems.

The resulting Nyquist plots were analyzed with ZView2 software using the above circuit, where R_s is the solution resistance and R_{ct} is the charge transfer resistance. CPE is the constant phase element.

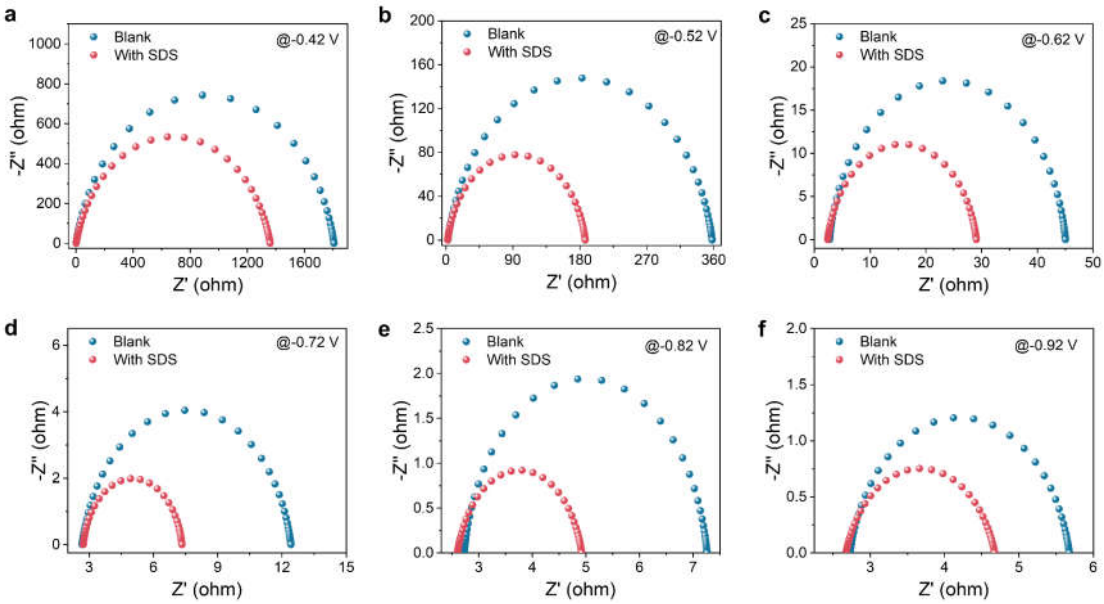

Figure S18. Nyquist plots of 0.1 M H_2SO_4 + 0.2 M K_2SO_4 electrolyte without (blank system) or with 0.4 mM SDS measured from –0.42 to –0.92 V vs. RHE.

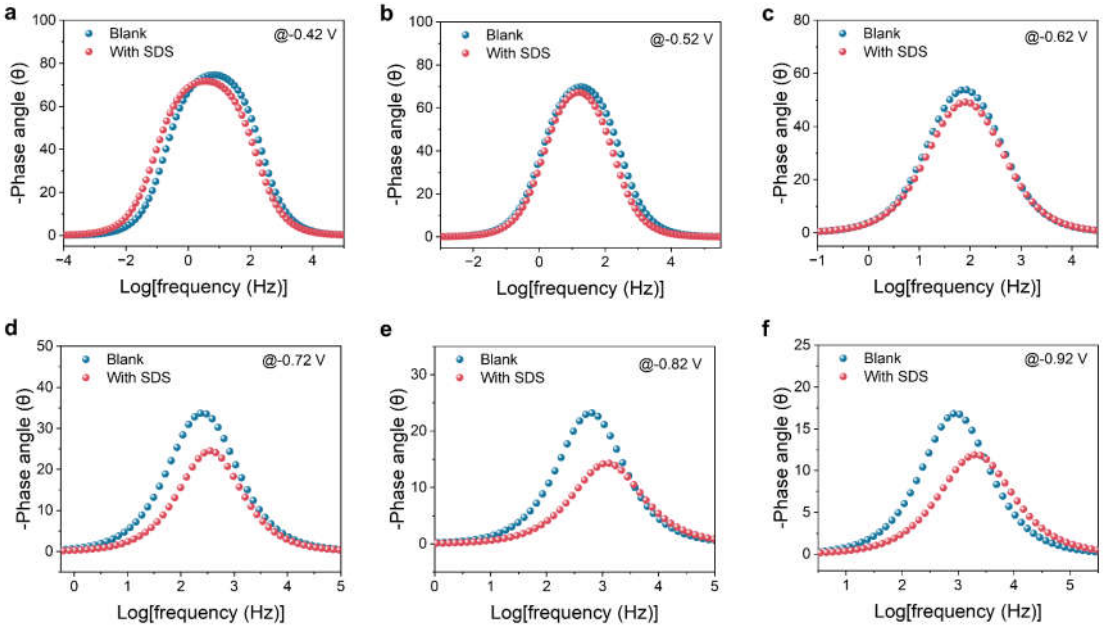

Figure S19. Bode plots of 0.1 M H_2SO_4 + 0.2 M K_2SO_4 electrolyte without (blank system) or with 0.4 mM SDS measured from –0.42 to –0.92 V vs. RHE.

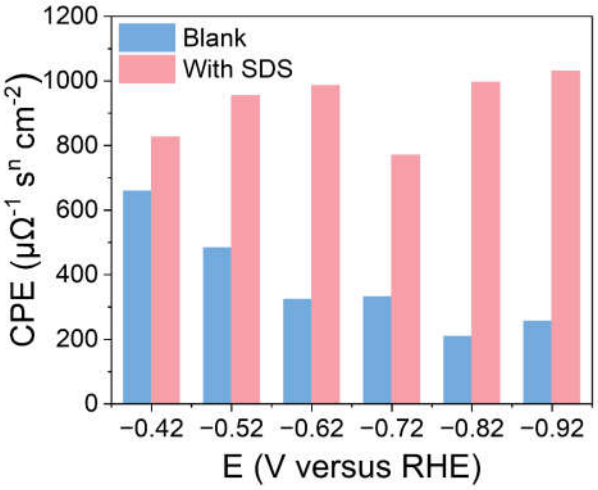

Figure S20. CPE values of the 0.1 M H_2SO_4 + 0.2 M K_2SO_4 electrolyte without/with 0.4 mM SDS measured by EIS.

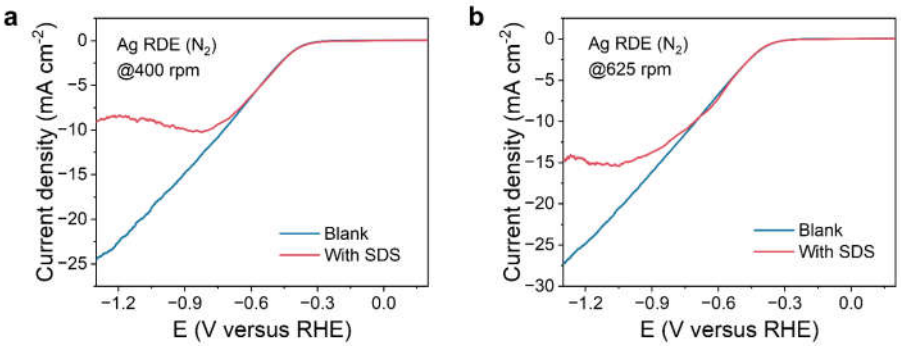

Figure S21. LSV curves of 0.1 M H_2SO_4 + 0.2 M K_2SO_4 electrolyte without/with 0.4 mM SDS under N_2 saturation, scanned at 50 mV s^{-1}. Rotation rates: (**a**) 400 rpm; (**b**) 625 rpm.

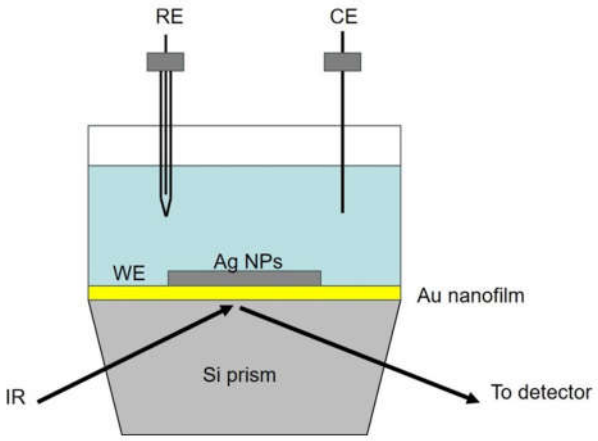

Figure S22. Schematic of in situ ATR-SEIRAS.

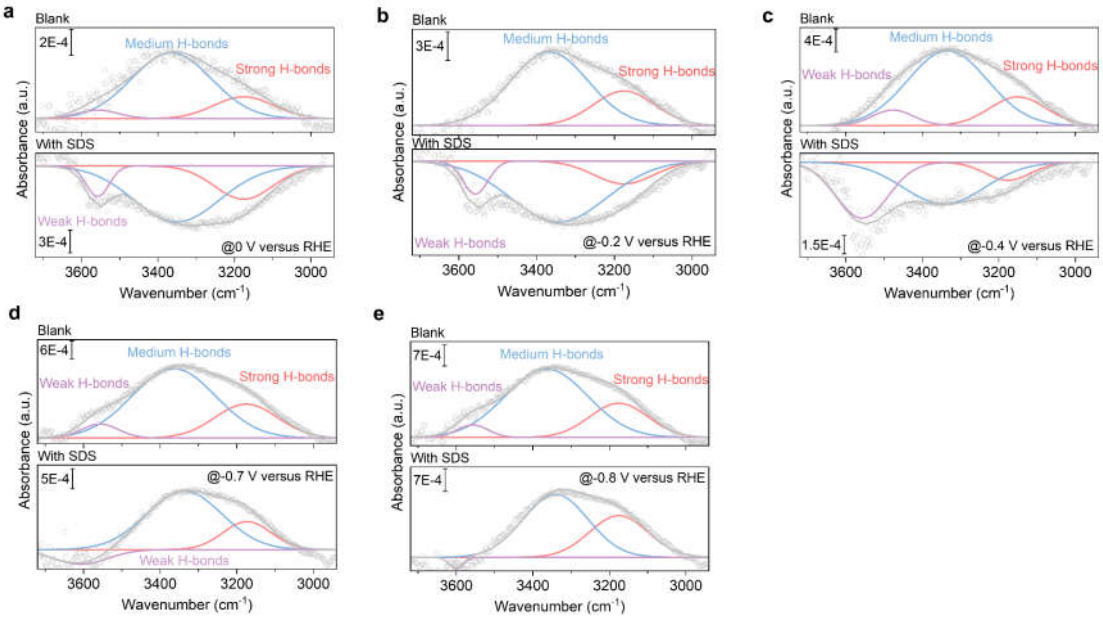

Figure S23. Deconvolution of ν_{OH} bands at diferent potentials for two systems.

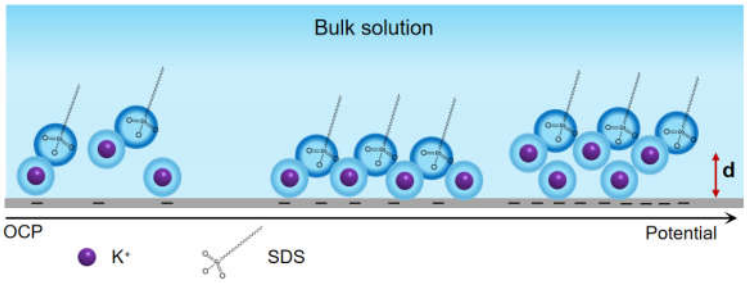

Figure S24. Schematic representation of the potential-dependent interfaces formed by anionic surfactants SDS.

From 0.2 V to -0.2 V, as the potential gradually increases, SDS anions are progressively adsorbed near the electrode surface under electrostatic interactions with cations, manifested by an intensified v-CH vibrational signal (**Figures 5d and 5e**). From -0.2 V to -0.8 V, further cathodic polarization enhances electrostatic repulsion between the electrode and anionic components, causing the composite solvation structures involving SDS molecules to retreat from the electrode surface—this correlates with diminished v-CH vibrational intensity and a broadened EDL structure. Given that practical reaction potentials operate at significantly more negative values than those tested via infrared spectroscopy, we propose that during electrolysis, the EDL adopts a loose configuration wherein SDS modulates local hydrogen-bond networks and spatial distribution of cationic concentrations.

2. Supplementary Tables:

Table S1. Simulated impedance of blank electrolyte system over Ag electrode at different potentials.

Potential (V versus RHE)	R_{ct} (Ω cm^{-2})	Y_0/CPE ($\mu\Omega^{-1}$ s^n cm^{-2})	n
-0.42	1804	658.89	0.877
-0.52	355.4	483	0.890
-0.62	42.34	322.94	0.911
-0.72	9.749	331	0.905
-0.82	4.533	208.71	0.902
-0.92	2.95	256	0.873

Table S2. Simulated impedance of SDS-containing electrolyte system over Ag electrode at different potentials.

Potential (V versus RHE)	R_{ct} (Ω cm^{-2})	Y_0/CPE ($\mu\Omega^{-1}$ s^n cm^{-2})	n
-0.42	1358	826	0.849
-0.52	184.9	955	0.883
-0.62	26.68	986	0.881
-0.72	4.604	771	0.901
-0.82	2.319	996	0.854
-0.92	2	1030.5	0.821

Table S3. Hydrogen evolution activity.

	Free energy (298.15 K, 0.1 M)	ΔG^{sol} (Hartree)	ΔG^{sol} (kJ mol^{-1})	ΔG^{sol} (kJ mol^{-1})
H_2O+H_2O	−152.917	0.590802	1551.1496	213.6067
H_2O+OH^-	−152.326			
$SDS+H_2O$	-1172.8	0.67216	1764.7563	
$SDS+OH^-$	-1172.12			